J|A|C|S ARTICLES

Published on Web 12/08/2009

Gold, Copper, and Platinum Nanoparticles Dispersed on $CeO_x/TiO_2(110)$ Surfaces: High Water-Gas Shift Activity and the Nature of the Mixed-Metal Oxide at the Nanometer Level

Joon B. Park,[†,‡] Jesus Graciani,[†,§] Jaime Evans,[||] Dario Stacchiola,[†,⊥] Sanjaya D. Senanayake,[†] Laura Barrio,[†] Ping Liu,[†] Javier Fdez. Sanz,[§] Jan Hrbek,[†] and José A. Rodriguez*[,†]

Chemistry Department, Brookhaven National Laboratory, Upton, New York 11973, Departamento de Química Física, Universidad de Sevilla, E-41012 Seville, Spain, and Facultad de Ciencias, Universidad Central de Venezuela, Caracas 1020 A, Venezuela

Received October 14, 2009; E-mail: rodrigez@bnl.gov

Abstract: At small coverages of ceria on $TiO_2(110)$, the CeO_x nanoparticles have an unusual coordination mode. Scanning tunneling microscopy and density-functional calculations point to the presence of Ce_2O_3 dimers, which form diagonal arrays that have specific orientations of 0, 24, and 42° with respect to the [1 −1 0] direction of the titania substrate. At high coverages of ceria on $TiO_2(110)$, the surface exhibits two types of terraces. In one type, the morphology is not very different from that observed at low ceria coverage. However, in the second type of terrace, there is a compact array of ceria particles with structures that do not match the structures of $CeO_2(111)$ or $CeO_2(110)$. The titania substrate imposes on the ceria nanoparticles nontypical coordination modes, enhancing their chemical reactivity. This phenomenon leads to a larger dispersion of supported metal nanoparticles (M = Au, Cu, Pt) and makes possible the direct participation of the oxide in catalytic reactions. The $M/CeO_x/TiO_2(110)$ surfaces display an extremely high catalytic activity for the water-gas shift reaction that follows the sequence $Au/CeO_x/TiO_2(110) < Cu/CeO_x/TiO_2(110) < Pt/CeO_x/TiO_2(110)$. For low coverages of Cu and CeO_x, $Cu/CeO_x/TiO_2(110)$ is 8−12 times more active than Cu(111) or Cu/ZnO industrial catalysts. In the $M/CeO_x/TiO_2(110)$ systems, there is a strong coupling of the chemical properties of the admetal and the mixed-metal oxide: The adsorption and dissociation of water probably take place on the oxide, CO adsorbs on the admetal nanoparticles, and all subsequent reaction steps occur at the oxide−admetal interface. The high catalytic activity of the $M/CeO_x/TiO_2(110)$ surfaces reflects the unique properties of the mixed-metal oxide at the nanometer level.

Introduction

Ceria (CeO_2) is an oxide with important applications in areas of catalysis, electrochemistry, photochemistry, and materials science.[1,2] In its most stable phase, bulk CeO_2 adopts a fluorite-type *Fm*3*m* crystal structure in which each metal cation is surrounded by eight oxygen atoms.[2,3] Experimental and theoretical studies indicate that ceria is best described as an ionocovalent compound or covalent insulator.[4,5] One of the most interesting properties of ceria is its ability to undergo facile conversion between "+4" and "+3" formal oxidation states.[2] Due to this property, ceria-containing catalysts exhibit a high performance in many chemical processes,[2] including the control of emissions of CO and NO_x from automobile exhaust, the destruction of SO_2, the hydrogenation of olefins, and the production of hydrogen through the water-gas shift reaction (WGS, $CO + H_2O \rightarrow H_2 + CO_2$).[6−14] The surface chemistry and catalytic properties of CeO_2 depend on the formation of

[†] Brookhaven National Laboratory.
[‡] Current address: Institute of Fusion Science, Department of Chemistry Education, Chonbuk National University, Jeonju, Jeonbuk 561-756, South Korea.
[§] Universidad de Sevilla.
[||] Universidad Central de Venezuela.
[⊥] Current address: Department of Chemistry, Michigan Technological University, Houghton, MI 49931.

(1) Thompson, A. M. *Oxides of the Rare Earths*; Wiley: New York, 1978.
(2) *Catalysis by Ceria and Related Materials*; Trovarelli, A., Ed.; World Scientific: London, 2002.
(3) Wyckoff, R. W. G. *Crystal Structures*, 2nd ed.; Wiley: New York, 1964.
(4) Marabelli, F.; Wachter, P. *Phys. Rev. B* **1987**, *36*, 1987.
(5) (a) Koelling, D. D.; Boring, A. M.; Wood, J. H. *Solid State Commun.* **1983**, *47*, 227. (b) Liu, G.; Rodriguez, J. A.; Chang, Z.; Hrbek, J.; Peden, C. H. F. *J. Phys. Chem. B* **2004**, *108*, 2931.
(6) (a) Gonzalez, I. D.; Navarro, R. M.; Alvarez-Galvan, M. C.; Rosa, F.; Fierro, J. L. G. *Catal. Commun.* **2008**, *9*, 1759. (b) Gonzalez, I. D.; Navarro, R. M.; Wen, W.; Marinkovic, N.; Rodríguez, J. A.; Rosa, F.; Fierro, J. L. G. *Catal. Today*, in press (http://dx.doi.org/10.1016/j.cattod.2009.07.100).
(7) Burch, R. B. *Phys. Chem. Chem. Phys.* **2006**, *8*, 5483.
(8) Fu, Q.; Saltsburg, H.; Flytzani-Stephanopoulos, M. *Science* **2003**, *301*, 985.
(9) (a) Panagiotopoulou, P.; Christodoulakis, A.; Kondarides, D. I.; Boghosian, S. *J. Catal.* **2006**, *240*, 114. (b) Panagiotopoulou, P.; Papavasiliou, J.; Avgouropoulos, G.; Ioannides, T.; Kondarides, D. I. *Chem. Eng. J.* **2007**, *134*, 16.
(10) Rodriguez, J. A.; Liu, P.; Hrbek, J.; Evans, J.; Perez, M. *Angew. Chem., Int. Ed.* **2007**, *46*, 1329.
(11) Rynkowski, J.; Farbotko, J.; Touroude, R.; Hilaire, L. *Appl. Catal., A* **2000**, *203*, 335.
(12) Gamarra, D.; Munuera, G.; Hungria, A. B.; Fernandez-Garcia, M.; Conesa, J. C.; Midgley, P. A.; Wang, X.; Hanson, J. C.; Rodriguez, J. A.; Martinez-Arias, A. *J. Phys. Chem. C* **2007**, *111*, 11026.

 10.1021/ja9087677

Ce^{3+} ions,[2] and different approaches are followed to maximize their concentration.[6–14]

In principle, the combination of two metals in a common oxide matrix can produce materials with novel structural and/or electronic properties.[3,15] In a recent study, we investigated the behavior of ceria nanoparticles in contact with $TiO_2(110)$ using scanning tunneling microscopy (STM), photoemission, and calculations based on density-functional theory (DFT).[16] For the $CeO_x/TiO_2(110)$ systems, the titania substrate imposes on the ceria nanoparticles nontypical coordination modes with a subsequent change in the relative stability of the Ce^{3+}/Ce^{4+} oxidation states that leads to a significant enhancement in chemical activity.[16] In this paper, we examine in more detail the growth mode and structure of the ceria nanoparticles supported on $TiO_2(110)$. Quite different surface structures or morphologies are found at low and high coverages of ceria. Isolated Ce_2O_x dimers are seen at low ceria coverages, while there is a massive transformation of the oxide surface structure at high coverages.

In the case of the WGS reaction, ceria is frequently used as a support for dispersing Au, Cu, and Pt particles.[6–8,17,18] In these catalysts, the ceria is not a simple inert support.[7,8,10] For example, surfaces of bulk metallic gold and nanoparticles of this metal interact weakly with water and cannot catalyze the WGS reaction.[19,20] Thus, without a direct participation of ceria in the catalytic process, it is very difficult to explain the high activity of $Au-CeO_2$ WGS catalysts.[7,8,20] However, if water dissociates on the oxide,[20] the subsequent steps of the WGS reaction (i.e., $OH(ads) + CO(ads) \rightarrow CO_2(ads) + 0.5H_2(gas)$) can take place on Au sites of the catalysts.[21] On the other hand, extended surfaces and nanoparticles of copper and platinum are able to catalyze the WGS reaction.[10,22–24] In fact, surfaces of copper have become benchmark systems for studying the WGS reaction.[19,23–25] Pt supported on ceria-modified powders of TiO_2 has shown a much better thermal stability and a higher WGS activity than Pt catalysts supported on either ceria or titania.[6] The structural or electronic properties responsible for the high performance of Pt/CeO_x-TiO_2 catalysts are not well understood.[6] It is important to note that ceria-modified TiO_2 is inactive for the WGS reaction.[16]

In this work, we present a systematic study of the structural, electronic, and catalytic properties of gold, copper, and platinum nanoparticles dispersed on $CeO_x/TiO_2(110)$. The special properties of $CeO_x/TiO_2(110)$ surfaces drastically affect the growth mode of the metal nanoparticles. In addition, there is a strong coupling of the chemical properties of the metal nanoparticles and the mixed-metal oxide. Gold is the metal most affected, but any of the investigated systems has a much higher WGS activity than Cu(111) or Cu/ZnO catalysts used in industrial applications.[23,24] The nature of the mixed-metal oxide at the nanometer level opens new directions for tuning catalytic activity.

Experimental and Theoretical Methods

A. Microscopy, Photoemission, and Catalytic Tests. The STM studies were performed in an Omicron ultrahigh-vacuum (UHV) chamber with a base pressure of less than 1.0×10^{-10} Torr. This chamber is equipped with a variable-temperature STM (VT-STM), low-energy electron diffraction (LEED), Auger electron spectroscopy (AES), a surface cleaning facility, gas leak valves, and metal evaporators. A more detailed description of this chamber is available elsewhere.[26,27] Experiments were carried out on a rutile $TiO_2(110)$ crystal purchased from Princeton Scientific Corp. The clean surface was prepared by Ne^+ ion sputtering at 1 kV for 30 min with an ion beam current of $\sim 3\ \mu A$, followed by annealing to 950 K for 5 min. The high-resolution STM images of the surface exhibited bright Ti rows separated by 6.5 Å, as typically observed for $TiO_2(110)$-(1×1).[28] Ce, Au, Cu, and Pt were deposited onto the $TiO_2(110)$ surface using metal evaporators.[10,16,29] The surface coverage of ceria and the admetals was estimated from the cluster height, diameter, and number density observed in the STM images, assuming the clusers have parabolic shape. All of the STM measurements were performed in constant current mode with positive sample biases of 0.4−2.8 V and tunneling currents of 0.4−0.7 nA using electrochemically etched tungsten tips. For in situ STM studies, the STM tip was moved 500 nm away from the direction of the metal flux in order to prevent the tip from shadowing the surface from incoming metal atoms.

Photoemission studies were performed at beamline U7A of the National Synchrotron Light Source (NSLS) at Brookhaven National Laboratory using a photon energy of 625 eV to collect the O 1s and Ti 2p regions and 325 eV to collect the Ce 4d, Au 4f, Pt 4f, and valence regions. In a separate UHV chamber, we acquired XPS spectra (Ce 3d, Ti 2p, O 1s, Au 4f, Cu 2p, and Pt 4f regions) and UPS spectra (valence region) using Mg Kα and He−I radiation, respectively. The core levels of Ce display quite different features for Ce^{3+} and Ce^{4+} oxidation states.[5b,20] Curve-fitting of the Ce 3d XPS spectra[20] allowed us to determine the ratio of Ce^{3+}/Ce^{4+} in the ceria overlayers. The area of the titania surface covered by ceria and the admetals was estimated using a combination of ion scattering spectroscopy (ISS) and photoemission.[16,20,29]

The catalytic studies were carried out in a system which combines a batch reactor and a UHV chamber.[10,20,29] The sample could be transferred between the reactor and UHV chamber without exposure to air. Typically, it was transferred to the batch reactor at $\sim$ 298 K; then the reactant gases were introduced (water-gas shift, 20 Torr of CO and 10 Torr of H_2O; CO oxidation, 4 Torr of CO and 2 Torr of O_2). The catalytic activity for the water-gas shift was

(13) Fang, J.; Bao, H.; He, B.; Wang, F.; Si, D.; Jiang, Z.; Pan, Z.; Wei, S.; Huang, W. *J. Phys. Chem. C* **2007**, *111*, 19078.
(14) Jacobs, G.; Williams, L.; Graham, U.; Thomas, G. A.; Sparks, D. E.; Davis, B. H. *Appl. Catal., A* **2003**, *252*, 107.
(15) Rodriguez, J. A. *Theor. Chem. Acc.* **2002**, *107*, 117; *Catal. Today* **2003**, *85*, 177.
(16) Park, J. B.; Graciani, J.; Evans, J.; Stacchiola, D.; Ma, S.; Liu, P.; Nambu, A.; Sanz, J. F.; Hrbek, J.; Rodriguez, J. A. *Proc. Natl. Acad. Sci. U.S.A.* **2009**, *106*, 4975.
(17) Li, Y.; Fu, Q.; Flytzani-Stephanopoulos, M. *Appl. Catal., B* **2000**, *27*, 179.
(18) Wang, X.; Rodriguez, J. A.; Hanson, J. C.; Gamarra, D.; Martínez-Arias, A.; Fernández-García, M. *J. Phys. Chem. B* **2006**, *110*, 428.
(19) Liu, P.; Rodriguez, J. A. *J. Chem. Phys.* **2007**, *126*, 164705.
(20) Rodriguez, J. A.; Ma, S.; Liu, P.; Hrbek, J.; Evans, J.; Pérez, M. *Science* **2007**, *318*, 1757.
(21) (a) Gong, J.; Ojifinni, R. A.; Kim, T. S.; Stiehl, J. D.; McClure, S. M.; White, J. M.; Mullins, C. B. *Top. Catal.* **2007**, *44*, 57. (b) Kim, T. S.; Gong, J.; Ojifinni, R. A.; White, J. M.; Mullins, C. B. *J. Am. Chem. Soc.* **2006**, *128*, 6282.
(22) Grabow, L. C.; Gokhale, A. A.; Evans, S. T.; Dumesic, J. A.; Mavrikakis, M. *J. Phys. Chem. C* **2008**, *112*, 4608.
(23) Nakamura, J.; Campbell, J. M.; Campbell, C. T. *J. Chem. Soc., Faraday Trans.* **1990**, *86*, 2725.
(24) Gokhale, A. A.; Dumesic, J.; Mavrikakis, M. *J. Am. Chem. Soc.* **2008**, *130*, 1402.
(25) Callaghan, C. A.; Vilekar, S. A.; Fishtik, I.; Datta, R. *Appl. Catal., A* **2008**, *345*, 213.
(26) (a) Song, Z.; Hrbek, J.; Osgood, R. *Nano Lett.* **2005**, *5*, 1327. (b) Song, Z.; Cai, T. H.; Hanson, J. C.; Rodriguez, J. A.; Hrbek, J. *J. Am. Chem. Soc.* **2004**, *126*, 8576.
(27) (a) Ma, S.; Zhao, X.; Rodriguez, J. A.; Hrbek, J. *J. Phys. Chem. C* **2007**, *111*, 3685. (b) Ma, S.; Rodriguez, J. A.; Hrbek, J. *Surf. Sci.* **2008**, *602*, 3272.
(28) (a) Park, J. B.; Conner, S. F.; Chen, D. A. *J. Phys. Chem. C* **2008**, *112*, 5490. (b) Diebold, U. *Surf. Sci. Rep.* **2003**, *48*, 53.
(29) Rodriguez, J. A.; Evans, J.; Graciani, J.; Park, J.-B.; Liu, P.; Hrbek, J.; Sanz, J. F. *J. Phys. Chem. C* **2009**, *113*, 7364.

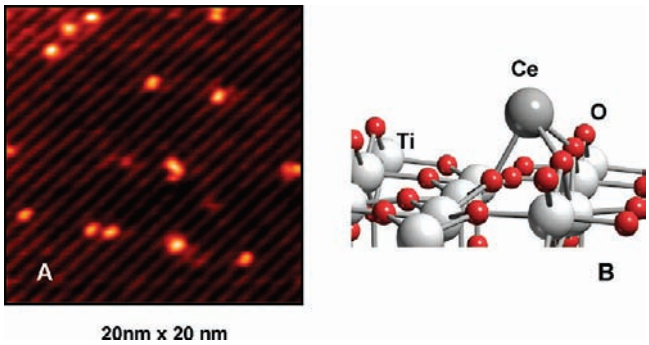

Figure 1. (A) STM image of Ce atoms deposited on a clean $TiO_2(110)$ surface at 298 K in UHV (V_t, 1.5 V; I_t, 0.05 nA). (B) Lowest energy structure obtained in DF calculations for the adsorption of a Ce atom on $TiO_2(110)$.

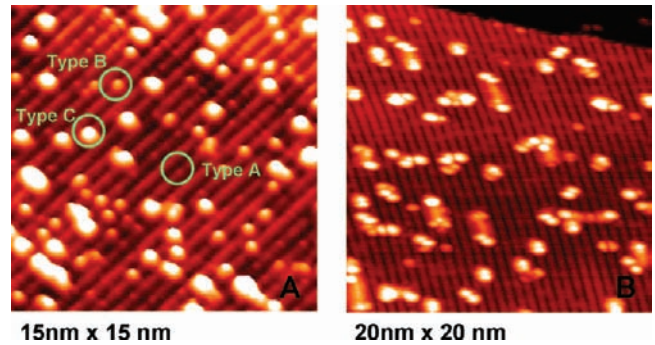

Figure 2. (A) STM image taken after the deposition of Ce atoms on a clean $TiO_2(110)$ surface under an O_2 atmosphere (P_{O_2}, 1.0×10^{-7} Torr) at room temperature (V_t, 1.7 V; I_t, 0.06 nA). The bright features are classified as types A−C on the basis of their apparent heights (see text). (B) STM image obtained after heating the surface in part A at 600 K for 10 min in UHV (V_t, 1.6 V; I_t, 0.07 nA).

measured at 625 K.[10,20,29] Product yields were analyzed by gas chromatography or mass spectroscopy.[20,23] The amount of molecules produced was normalized by the active area exposed by the sample. In our reactor a steady-state regime for the water-gas shift or the oxidation of CO was reached after 2−3 min of reaction time.

B. Density Functional Calculations. Periodic DFT calculations using a GGA+U exchange-correlation potential were performed using the VASP code[30] with a (4 × 2) six-layer-thick supercell to model the $TiO_2(110)$ surface.[16,31] The adlayer and first four layers of the titania slab were allowed to relax during the DFT geometry optimizations. We used the Perdew−Wang 91 GGA functional for exchange correlation, the projector-augmented wave approach, and plane waves with a cutoff energy set at 400 eV. We treated the Ti(3s,3p,3d,4s), Ce(4f,5s,5p,5d,6s), and O(2s,2p) electrons as valence states, while the remaining electrons were kept frozen as core states.[16,31] The calculations were performed at the Γ point of the Brillouin zone.[30] To reproduce the valence spectra of Ce/$TiO_2(110)$, we utilized U_{eff} parameters with a value of 4.5 eV for Ce and Ti.[16] This value is close to those used in previous studies for bulk ceria or titania.[32,33] The introduction of the U_{eff} parameters in the DFT calculations was found to be essential to correctly reproduce the position of the occupied Ce 4f and Ti 3d levels in the valence region of $CeO_x/TiO_2(110)$,[16] even though the trends found in the energetics for the coadsorption of Ce and O on $TiO_2(110)$ were almost the same with or without the U_{eff} parameters.

Results

A. Structures of CeO_x on $TiO_2(110)$. Less than 0.1 monolayer of Ce atoms was deposited on a clean $TiO_2(110)$ surface at room temperature in UHV to investigate the interactions between Ce and titania; see Figure 1A. The bright spots are evenly distributed on the terrace without an apparent preference to the steps, and their average height was determined to be 1.4 ± 0.2 Å. In measurements of XPS and UPS (data not shown),[16] the oxidation state of the Ti cations changed from +4 to +3 and Ce was found in a +3 oxidation state. The adsorption of Ce partially reduced the TiO_2 surface by donating electrons to Ti cations. Since the Ce atoms most likely interact with surface O anions rather than Ti cations, we correlated the bright spots in Figure 1A to CeO_x species on $TiO_2(110)$. Figure 1B displays the calculated adsorption geometry for a Ce adatom. On its most stable adsorption site, Ce interacts with two bridging and one in-plane O atom of the $TiO_2(110)$ surface. This type of bonding configuration is consistent with our images of STM. Since the heats of formation of cerium oxides are larger than those of titanium oxides,[34] the titania substrate is forced to share its oxygens with the Ce adatoms. The calculated oxidation state for Ce is 3+, in perfect agreement with the experiment. The fact that three electrons move from high to lower energy levels, $Ce(5d^16s^2) \rightarrow 3Ti(3d^1)$, leads to a very high adsorption energy (−7.23 eV) for Ce on $TiO_2(110)$.

The presence of O_2 in the background drastically affected the growth mode of ceria and the morphology of the surface. In Figure 2A, Ce atoms were deposited at room temperature under an atmosphere of O_2 ($\sim 1 \times 10^{-7}$ Torr) to avoid the surface reduction of the titania substrate. Three different types of new features were found, nonrelated to the ideal $TiO_2(110)$ surface, which were designated as type A, type B, and type C based on their apparent heights (type A, 0.3 ± 0.1 Å; type B, 1.3 ± 0.2 Å; type C, 1.9 ± 0.3 Å). The type A (tiny bright spots) can be correlated with oxygen adatoms (O_{ad}). Several recent publications have showed O_2 dissociation on O vacancies of $TiO_2(110)$, and we also confirmed their results in a separate control experiment (data not shown).[35−37] Upon O_2 exposure to the surface, an O_2 molecule can be dissociated at the bridging oxygen vacancy in two oxygen adatoms. One oxygen atom heals the vacancy, and the other is deposited on Ti atomic rows, which appear to be tiny bright spots in STM images. The type B (bright spots) can be attributed to CeO_x, after comparison with the shape and height of the bright spots in Figure 1A. Finally, the type C features (very bright spots) correspond to TiO_x islands on $TiO_2(110)$ induced by O_2 chemisorption.[38] They are a consequence of the migration of Ti interstitials from the bulk to the surface of the titania crystal induced by oxygen adatoms. The morphological shape and reported height of the type C features (2.2 Å) are very close to our observations.[38]

(30) Kresse, G.; Furthmuller, J. *Comput. Mater. Sci.* **1996**, *6*, 15.
(31) (a) Graciani, J.; Nambu, A.; Evans, J.; Rodriguez, J. A.; Sanz, J. F. *J. Am. Chem. Soc.* **2008**, *130*, 12056. (b) Graciani, J.; Alvarez, L. J.; Rodriguez, J. A.; Sanz, J. F. *J. Phys. Chem. C* **2008**, *112*, 2624.
(32) Fabris, S.; de Gironcoli, S.; Baroni, S.; Vicario, G.; Balducci, G. *Phys. Rev. B* **2005**, *71*, 041101.
(33) Zhang, C.; Michaelides, A.; King, D. A.; Jenkins, S. J. *J. Chem. Phys.* **2008**, *129*, 194708.
(34) *Lange's Handbook of Chemistry*, 13th ed.; Dean J. A., Ed.; McGraw-Hill: New York, 1985; Table 9.
(35) Du, Y. G.; Deskins, N. A.; Zhang, Z. R.; Dohnalek, Z.; Dupuis, M.; Lyubinetsky, I. *J. Phys. Chem. C* **2009**, *113*, 666, and references therein.
(36) Zhang, Z.; Du, Y.; Petrik, N. G.; Kimmel, G. A.; Lyubinetsky, I.; Dohnalek, Z. *J. Phys. Chem. C* **2009**, *113*, 1908.
(37) Wendt, S.; Schaub, R.; Matthiesen, J.; Vestergaard, E. K.; Wahlstrom, E.; Rasmussen, D.; Thostrup, P.; Molina, L. M.; Laegsgaard, E.; Stensgaard, I.; Hammer, B.; Besenbacher, F. *Surf. Sci.* **2005**, *598*, 226.
(38) Wendt, S.; Sprunger, P. T.; Lira, E.; Madsen, G. K. H.; Li, Z. S.; Hansen, J. O.; Matthiesen, J.; Blekinge-Rasmussen, A.; Laegsgaard, E.; Hammer, B.; Besenbacher, F. *Science* **2008**, *320*, 1755.

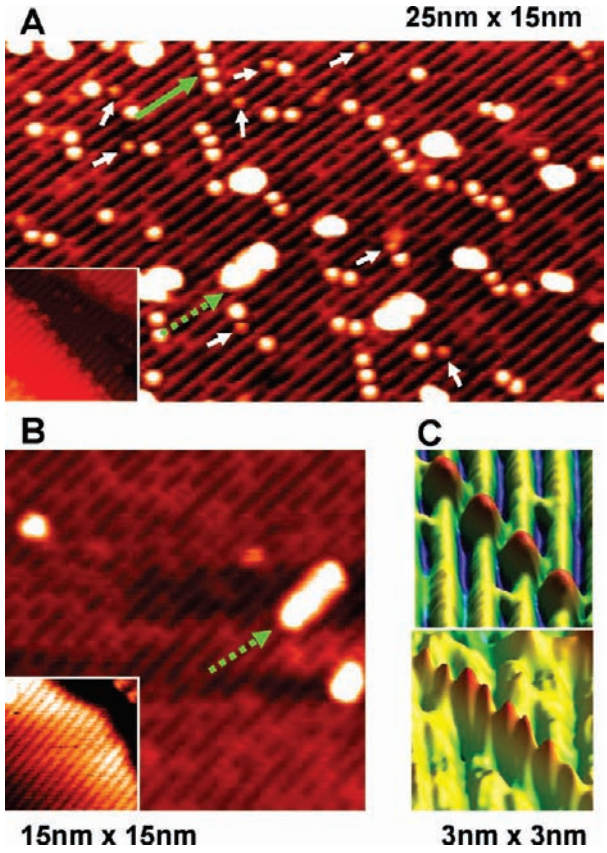

Figure 3. (A) STM image of CeO_x on the $TiO_2(110)$ surface after depositing Ce atoms at 600 K in O_2 (P_{O_2}, 1×10^{-7} Torr) and subsequent annealing at 900 K in O_2 (P_{O_2}, 1×10^{-4} Torr; V_t, 1.2 V; I_t, 0.07 nA). (B) STM image of a clean $TiO_2(110)$ surface after dosing O_2 (P_{O_2}, 1×10^{-4} Torr) to the sample at 750 K and subsequent annealing at 900 K. Insets in A and B show magnified STM images at the steps of each surface (V_t, 1.1 V; I_t, 0.06 nA). (C) Bias-dependent STM images of a diagonal array of CeO_x nanoparticles taken at the imaging bias of 1.2 V, 0.06 nA (top) and 0.4 V, 0.06 nA (bottom). Ce atoms were dosed at 600 K in O_2 (P_{O_2}, 5×10^{-5} Torr), and subsequently the sample was annealed to 900 K.

Figure 2B shows an STM image recorded after heating the surface in Figure 2A at 600 K for 10 min in UHV. The type A features due to O adatoms disappeared, and there was an agglomeration of the individual CeO_x nanoparticles (type B features) and TiO_x clusters (type C features) into bigger clusters. The number density of the nanoparticles decreased by ~70%. This result suggests that CeO_x particles are mobile at elevated temperature, and deficiency of O_2 leads to disordered surface structures of CeO_x, implying that oxygen atoms play an important role in the formation of ceria−titania mixed oxides.

On the basis of the results in Figure 2, we decided to prepare the $CeO_x/TiO_2(110)$ surfaces at high temperature. Ce was deposited on the titania surface at 600 K in O_2 ($\sim 1 \times 10^{-7}$ Torr), and the sample was subsequently annealed to 900 K still under an O_2 environment. The images in Figure 3 were taken after cooling the sample to room temperature and removing the O_2 from the background. Two different types of features were observed on the terraces: diagonal arrays of small bright spots (see solid arrow) and bigger ones (see dashed green arrow). To assign these features, a control experiment was performed by repeating the same experiment without depositing Ce on the surface (Figure 3B). From the control experiment, the bigger clusters in Figure 3A can be correlated with TiO_x islands, which resulted from reaction of oxygen gas with interstitial Ti from the reduced bulk.[38] The height of the TiO_x islands now increased

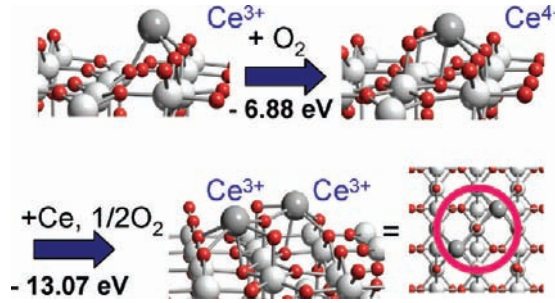

Figure 4. Most stable geometries and energy changes (ΔE) for the formation of a Ce_2O_3 dimer on $TiO_2(110)$. The top view of the surface Ce_2O_3 dimer is also shown for comparison with the model obtained from the STM images. Colors: white (Ti); dark gray (Ce); red (O).

to 3 Å, which is close in height to one atomic step on the TiO_2 surface and comparable to the results in refs 38 and 39. Now we can easily correlate diagonal arrays with CeO_x nanoparticles. The average height is 1.4 Å, which is close to the average height we obtained in Figures 1A and 2 for the CeO_x features.

The insets in Figure 3 show STM images at the steps, indicating that the CeO_x nanoparticles also decorated these surface sites. A very interesting observation in Figure 3A is that the relatively small CeO_x nanoparticles (short white arrows) with a height around 1.2 Å do not form diagonal arrays and are mostly located at the end of diagonal arrays or isolated on the terrace. To better understand the structures of the CeO_x nanoparticles, a bias-dependent STM measurement was performed, as shown in Figure 3C. These two images display the same diagonal arrays of CeO_x nanoparticles but obtained at different imaging bias. The top STM image was taken with an imaging bias of +1.2 V, and the angle of the diagonal array is close to 42° with respect to the [1 −1 0] direction. When this feature was imaged at +0.4 V, the individual bright features appeared as dimers. Each ceria dimer is located between two rows of oxygens protruding from the surface. Ce 3d XPS spectra indicated that the oxidation state of the Ce atoms in the dimers was essentially +3. On the other hand, in the Ti 2p XPS region we saw mainly Ti^{4+} with a small amount (<5%) of Ti^{3+} comparable to that found on clean $TiO_2(110)$.[28b] Thus, the presence of O_2 in the background during the deposition of Ce did prevent the reduction of the titania support.

Using DFT calculation, we investigated the bonding configuration of the ceria dimers on $TiO_2(110)$, as shown in Figure 4. Starting with the structure in Figure 1B, the dissociation of an O_2 molecule near the adsorbed Ce is a highly exothermic process and an energy of 6.88 eV is released. At this point, the oxidation state of Ce is +4. If a second Ce atom is deposited on this surface, the CeO_2 monomer would be an excellent binding site to create a dimer since one of the three electrons released by the new adatom does not go to a high-energy 3d level of Ti but rather goes to the 4f level of the first Ce atom. The second cerium either goes next to the ceria nanoparticle by sharing two oxygens, forming a horizontal dimer, or to a diagonal position by sharing one oxygen and bonding an extra oxygen atom, forming a diagonal dimer. The DFT calculations indicate that the diagonal dimer has a formation energy 2.6 eV more exothermic than the formation energy of the horizontal dimer. At the end, the ceria dimer adopts a configuration

(39) (a) Li, M.; Hebenstreit, W.; Diebold, U. *Phy. Rev. B* **2000**, *61*, 4926. (b) Li, M.; Hebenstreit, W.; Gross, L.; Diebold, U.; Henderson, M. A.; Jennison, D. R.; Schultz, P. A.; Sears, M. P. *Surf. Sci.* **1999**, *437*, 173.

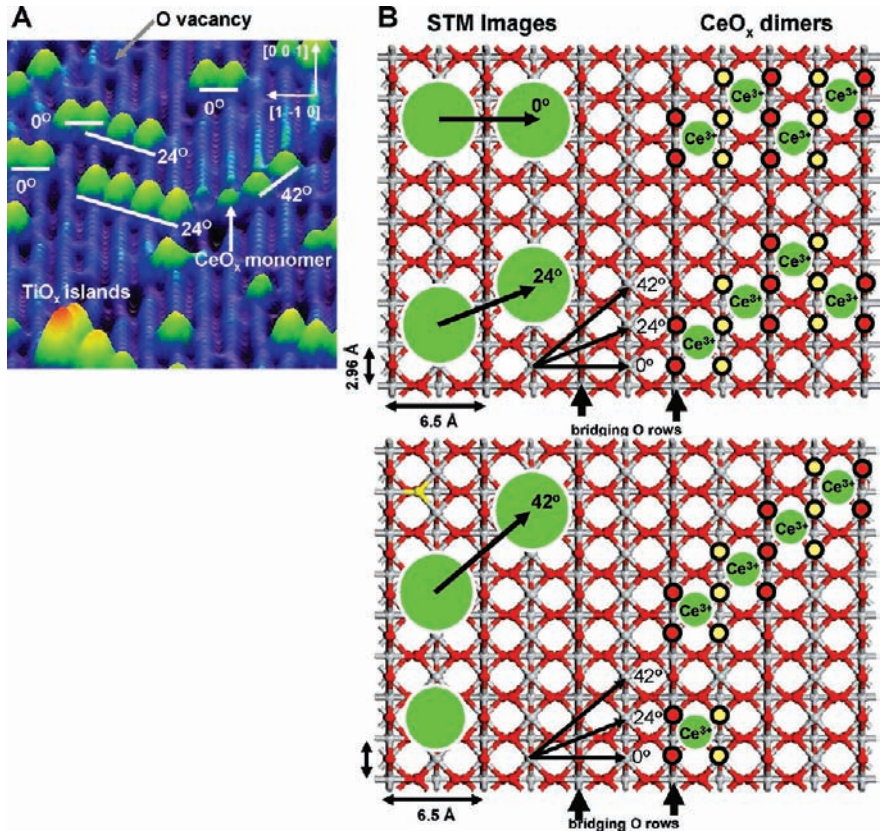

Figure 5. (A) High-resolution STM image for a low coverage of CeO_x on TiO_2(110). (B) Ball models for the arrays of CeO_x nanoparticles on the titania surface. Here, we are showing possible orientations of the CeO_x dimers based on the bias-dependent STM images, XPS, and DFT results (see text for more details).

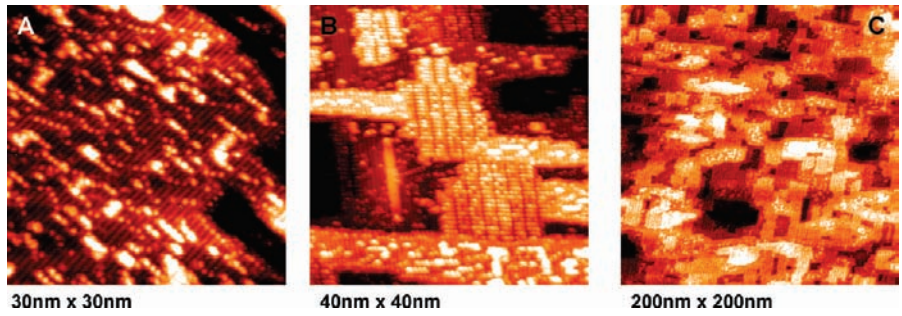

Figure 6. STM images obtained after depositing 0.7 monolayer of Ce atoms on TiO_2(110) at 600 K in O_2 and subsequent annealing at 900 K in O_2 (P_{O_2}, 1.0×10^{-7} Torr; V_t, 1.1 V; I_t, 0.06 nA): (A) an area having a morphology similar to that obtained for low coverages of ceria on titania; (B) an area having a higher coverage of Ce adatoms where the CeO_x nanoparticles form rectangular domains; (C) overview of a 200 nm × 200 nm region of the CeO_x/TiO_2(110) surface.

comparable to STM images in Figure 4C and have an oxidation state of +3, without the generation of Ti^{3+} species, as seen in the XPS measurements.

On the basis of our STM, XPS, UPS, and DFT results, we can construct a model for diagonal arrays of CeO_x nanoparticles on TiO_2(111) (Figure 5). The big bright spots are TiO_x islands, as we discussed in Figure 3A,B. Each bright spot from the diagonal arrays of CeO_x nanoparticles corresponds to one CeO_x dimer. The diagonal arrays of CeO_x have specific orientations of 0, 24, and 42° with respect to the [1 −1 0] direction. These angles exactly match the diagonal angles of zero, one, and two unit cells of TiO_2(110). When the diagonal angle is 0°, four cerium atoms will be oriented like a zigzag by sharing seven bridging oxygen atoms (red circles) and six newly bonded oxygen atoms to Ti atomic rows (yellow circles). 42° with respect to the [1, −1, 0] direction would have a linear distribution of cerium atoms sharing a total of 13 oxygen atoms. Likewise we can build 24° diagonal arrays of CeO_x nanoparticles as well. The relatively small CeO_x nanoparticles that are located at the end of diagonal arrays or isolated are probably CeO_x monomers since they are in lack of additional Ce atoms to share neighboring oxygens.

At high coverages of ceria on TiO_2(110), the STM images showed quite complex structures and a morphology very different from that of the titania substrate. Typical results are shown in Figure 6. The CeO_x/TiO_2(110) surface exhibits two types of terraces. In one type (Figure 6A), one has a morphology that is not very different from that observed in Figures 3 and 5 with linear arrays of ceria dimers and TiO_x clusters. However, in the second type of terrace (Figure 6B), there is a compact

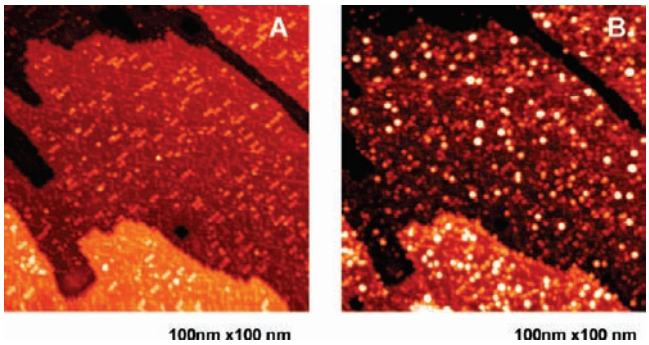

Figure 7. STM images of the same area before ((A) V_t, 1.6 V; I_t, 0.08 nA) and after ((B) V_t, 2.1 V; I_t, 0.07 nA) depositing Cu on a $CeO_x/TiO_2(110)$ surface at 300 K.

array of ceria particles with structures that do not match the structures of $CeO_2(111)$ or $CeO_2(110)$. At high coverages of ceria, one can speculate that all of the Ce adatoms cannot generate diagonal arrays of CeO_x nanoparticles due to the limited surface area of $TiO_2(110)$. They are forced to share the oxygens with next neighboring Ce adatoms, producing rectangular arrays of CeO_x nanoparticles (Figure 6B). The terraces in Figure 6A,B alternate in a complex way, and titania surfaces with a high coverage of ceria had a very rough morphology (Figure 6C). As the fraction of the titania covered by ceria increased from 0.3 to 0.7 (as measured by ISS), the line shape of the corresponding Ce 3d XPS spectra pointed to a changing mixture of Ce^{3+} (80−40%) and Ce^{4+} (20−60%). In general, Ce^{3+} was the dominating cation only at low or medium coverages of ceria.

B. Deposition of Au, Cu, and Pt Nanoparticles on $CeO_x/TiO_2(110)$. Previous studies have examined the growth mode of Au, Cu, and Pt nanoparticles on clean $TiO_2(110)$.[28,29,40] On this surface, the metals grow forming three-dimensional particles. Gold exhibits very weak interactions with the ideal terraces of the titania surface[29] and mainly binds to defects or step sites.[28a,40] Cu and Pt interact well with $TiO_2(110)$[29,41] and disperse on terraces of the surface.[28,29] In the case of $Pt/TiO_2(110)$, encapsulation of the Pt particles by TiO_x clusters is observed upon annealing to temperatures above 700 K.[28,42]

In this work, we investigated the deposition of Au, Cu and Pt nanoparticles on $TiO_2(110)$ surfaces partially (10−15%) covered with ceria, which are relevant for applications in catalysis.[6] These $CeO_x/TiO_2(110)$ systems were prepared following the procedure used to obtain the surface shown in Figure 3A. Our results of XPS indicated that the Au, Cu, and Pt nanoparticles remained in a metallic state after their deposition on the $CeO_x/TiO_2(110)$ surfaces. Figure 7 shows STM images acquired before and after depositing ~0.1 monolayer of Cu on a $CeO_x/TiO_2(110)$ surface at 300 K. The same region was imaged in situ to identify the nucleation sites of Cu. As discussed above, Figure 5A, the oxide surface exposes CeO_x nanoparticles and TiO_x clusters. Each of these has a particular height and configuration on the $TiO_2(110)$ substrate. In Figure 7B, Cu particles are distributed randomly on terraces, nucleating on both TiO_x islands and CeO_x nanoparticles. The average Cu cluster height is 0.3 ± 0.1 nm. Apparently, the Cu atoms do not migrate on the oxide surface to form relatively big Cu nanoparticles; instead they are trapped at TiO_x and CeO_x sites.

(40) Valden, M.; Lai, X.; Goodman, D. W. *Science* **1998**, *281*, 1647.
(41) Iddir, H.; Öğüt, S.; Browning, N. D.; Disko, M. M. *Phys. Rev. B* **2005**, *72*, 081407(R). *Phys. Rev. B*, **2006**, *73*, 039902(E).
(42) Dulub, O.; Heberstreit, W.; Diebold, U. *Phys. Rev. Lett.* **2000**, *84*, 3646.

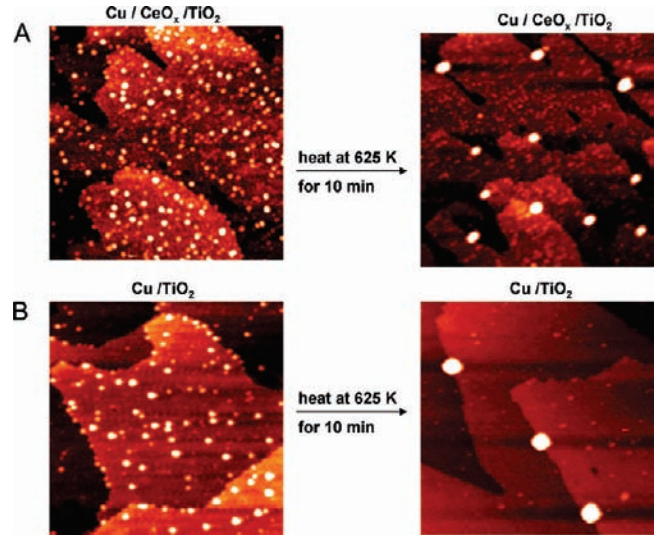

Figure 8. STM images obtained before and after heating metal/oxide surfaces at 625 K for 10 min: (A) 0.1 monolayer of Cu on $CeO_x/TiO_2(110)$ (V_t, 2.1 V; I_t, 0.06 nA); (B) 0.1 monolayer of Cu on $TiO_2(110)$ (V_t, 2.3 V; I_t, 0.04 nA). The Cu was deposited on the oxide surfaces at 300 K.

In Figure 8, we compare the morphologies obtained after depositing 0.1 monolayer of Cu on $CeO_x/TiO_2(110)$ and $TiO_2(110)$ surfaces at 300 K with subsequent annealing at 625 K for 10 min. At room temperature, the Cu particles are well-dispersed on the terraces of $TiO_2(110)$ and clearly there is no preference for nucleation on the steps. The average Cu cluster height is 0.5 ± 0.2 nm. This is higher than the average height of 0.3 ± 0.1 nm found for the same Cu coverage on the $CeO_x/TiO_2(110)$ surface at 300 K. Thus, the presence of CeO_x favors the dispersion of Cu on the oxide support: The size of the admetal particles decreases, and there is a larger number of these particles on the terraces. Upon annealing to 625 K, one sees the formation of large Cu particles at the step sites of the $Cu/CeO_x/TiO_2(110)$ and $Cu/TiO_2(110)$ systems. The large Cu particles in $Cu/TiO_2(110)$ have an average height of 2.3 nm and a diameter of 10.9 nm. In the case of $Cu/CeO_x/TiO_2(110)$, the large Cu particles have an average height of 0.9 nm and a diameter of 5.5 nm. Again the CeO_x favors the dispersion of Cu, and a substantial number of Cu particles remain on the terraces of $Cu/CeO_x/TiO_2(110)$ at 625 K.

The trends seen in Figures 7 and 8 for $Cu/CeO_x/TiO_2(110)$ are similar to those found after depositing 0.1 monolayer of Au on $CeO_x/TiO_2(110)$.[16] The CeO_x sites were essential for the nucleation of small particles of Au on terraces of the oxide support.[16] In the opposite extreme, we have Pt which binds well to terrace sites of $TiO_2(110)$.[28,41] Figure 9 shows STM images collected after depositing 0.1 monolayer of Pt on $CeO_x/TiO_2(110)$ at 300 K (part A) followed by annealing at 625 K (part B). The dispersion of the Pt particles is quite high at room temperature. It decreases upon heating to 625 K, but it remains much higher than that seen for Cu nanoparticles (Figure 8) or Au nanoparticles[16] under similar conditions. The average height of the Pt nanoparticles in Figure 9B is 0.6 nm and the diameter 4.5 nm.

We also investigated the deposition of Au, Cu, and Pt on $TiO_2(110)$ surfaces precovered with large coverages of ceria, as seen in Figure 6. In these systems, the CeO_x provides a big diversity of nucleation sites not found in the case of $TiO_2(110)$.

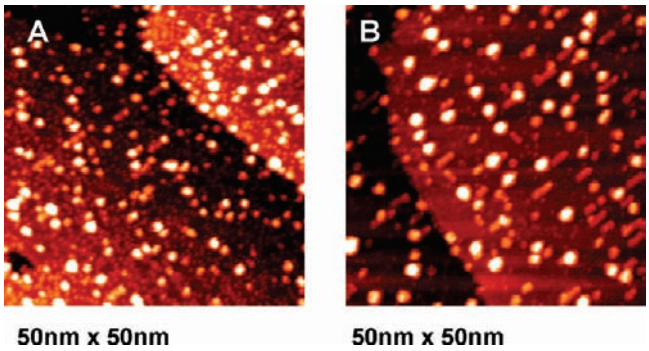

Figure 9. STM images taken before ((A) V_t, 2.1 V; I_t, 0.05 nA) and after ((B) V_t, 1.2 V; I_t, 0.05 nA) heating 0.1 monolayer of Pt on a $CeO_x/TiO_2(110)$ surface at 625 K for 10 min. The Pt was deposited on $CeO_x/TiO_2(110)$ at 300 K.

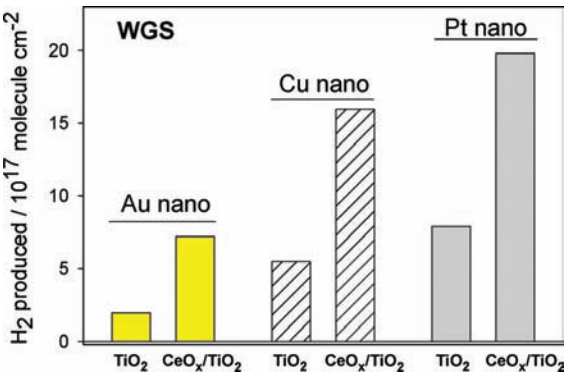

Figure 10. Amount of H_2 produced by the WGS reaction on catalysts generated by depositing 0.15 monolayer of Au, Cu, or Pt on $CeO_x/TiO_2(110)$ surfaces in which 12−14% of the titania was precovered with CeO_x nanoparticles. For comparison, we also include data for the deposition of the metals on $TiO_2(110)$. The reported values for the production of H_2 were obtained after exposing the catalysts to 20 Torr of CO and 10 Torr of H_2O at 625 K for 5 min. The number of H_2 molecules produced is normalized by the sample surface area.

However, they will not be discussed here, since they are of limited interest for catalytic applications,[6] as we will show below.

C. Water-Gas Shift Reaction on $M/CeO_x/TiO_2(110)$ (M = Au, Cu, Pt) Surfaces. The developing of new catalysts for the water-gas shift (WGS) reaction is critical for the production of pure hydrogen gas.[6–8] Many studies have tested the catalytic activity of metal nanoparticles supported on TiO_2 and CeO_2.[6–14,17,18] We have found that $TiO_2(110)$,[29] $CeO_2(111)$,[10] and $CeO_x/TiO_2(110)$[16] are not able to catalyze the WGS reaction. Water readily dissociates on the O vacancies of these oxide surfaces, but, upon reaction of adsorbed OH with CO, very stable formate (HCOO) or carbonate (CO_3) species are produced which make it very difficult to establish a catalytic cycle.[10,29] The dispersion of Cu nanoparticles on $TiO_2(110)$ and $CeO_2(111)$ produces excellent WGS catalysts which have similar activities with the one for $Cu/TiO_2(110)$ being slightly higher.[19,20,43] What happens when $CeO_x/TiO_2(110)$ is used as a support for metal nanoparticles during the WGS?

Figure 10 shows the amount of H_2 produced by the WGS reaction on catalysts generated by depositing 0.15 monolayer of Au, Cu, or Pt on $CeO_x/TiO_2(110)$ surfaces in which 12−14% of the titania was precovered with CeO_x nanoparticles. For comparison, we also include the corresponding data for the deposition of 0.15 monolayer of the admetals on plain $TiO_2(110)$. It is clear that the nature of the oxide support strongly affects the catalytic activity. The catalysts containing $CeO_x/TiO_2(110)$ display an activity that is 2.5−3.8 times higher than those containing plain $TiO_2(110)$[29] or $CeO_2(111)$.[10] When compared to Cu(111), a typical benchmark in studies of the WGS,[23–25] or Cu/ZnO, a common WGS catalyst for industrial applications,[7,10,23] the $M/CeO_x/TiO_2(110)$ systems are 5−15 times more active. The catalytic activity increases following the sequence: $Au/CeO_x/TiO_2(110) < Cu/CeO_x/TiO_2(110) < Pt/CeO_x/TiO_2(110)$. Although Au is the admetal with the lowest catalytic activity in Figure 10, it is the one most affected by coupling to $CeO_x/TiO_2(110)$, because neither extended surfaces of Au nor Au nanoparticles are able to catalyze the WGS.[19] The behavior of $Cu/CeO_x/TiO_2(110)$ is remarkable. Supported copper exhibits a WGS activity somewhat smaller than that of Pt, but it is much less expensive.

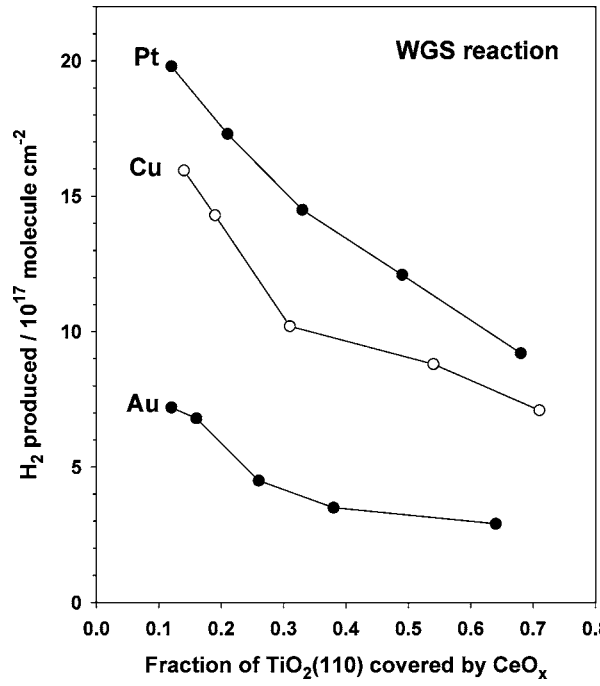

Figure 11. Effect of ceria coverage on the WGS activity of $M/CeO_x/TiO_2(110)$ (M = Au, Cu, Pt) catalysts. The catalysts were generated by depositing 0.15 monolayer of the admetals on the $CeO_x/TiO_2(110)$ surfaces. The reported values for the production of H_2 were obtained after exposing the catalysts to 20 Torr of CO and 10 Torr of H_2O at 625 K for 5 min. The number of H_2 molecules produced is normalized by the sample surface area.

Figure 11 displays the catalytic activity of the $M/CeO_x/TiO_2(110)$ systems ($\Theta_M \sim 0.15$ monolayer) as a function of the fraction of $TiO_2(110)$ covered by CeO_x. For the three admetals, an increase in the amount of CeO_x present in the oxide surface leads to a reduction in the catalytic activity. At the lowest coverages of CeO_x (12−14% of the titania covered), postreaction surface analysis with XPS[20] showed that only Ce^{3+} cations were present in the oxide support. In contrast, for the largest coverages of ceria (64−71% of the titania covered), postreaction surface analysis gave a mixture of Ce^{3+} and Ce^{4+} cations in the Ce 3d XPS spectra, and after curve-fitting[20] we found that the ratio $Ce^{3+}/Ce^{4+} \sim 0.45$. As the ceria overlayer adopts a more compact structure, see Figure 6, and a higher cerium oxidation state, +4, the catalytic activity of the $M/CeO_x/TiO_2(110)$ systems decreases and gets closer to that seen for the metals on $CeO_2(111)$.[10]

(43) Rodriguez, J. A.; Liu, P.; Wang, X.; Wen, W.; Hanson, J.; Hrbek, J.; Pérez, M.; Evans, J. *Catal. Today* **2009**, *143*, 45.

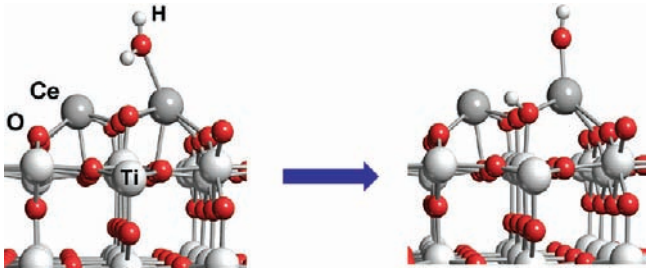

Figure 12. Initial and final geometries for the dissociation of a H_2O molecule on $Ce_2O_3/TiO_2(110)$. The corresponding reaction energy is −0.7 eV with an activation barrier of only 0.04 eV.

For the unsupported metals, the WGS activity increases in the following order: Au ≪ Pt < Cu,[19,22–24] a trend that does not match the ones seen in Figures 10 and 11. In principle, the oxide substrate can modify the chemical properties of the supported nanoparticles and/or participate directly in the WGS reaction. Theoretical calculations show a very weak interaction of Au with $TiO_2(110)$ and a negligible charge transfer.[29,44] Stronger electronic perturbations are observed for Au on $CeO_2(111)$[45] and for Cu and Pt on $TiO_2(110)$.[29,41] The ceria nanoparticles in Figures 3 and 5 interact well with admetals and improve their dispersion on the titania surface. For the $M/CeO_x/TiO_2(110)$ systems in Figure 10, the average height and diameter of the metal particles have a reverse order with respect to the catalytic activity [$Pt/CeO_x/TiO_2$ (H,0.6 nm; D, 4.5 nm) < $Cu/CeO_x/TiO_2$ (H, 0.9 nm; D, 5.5 nm) < $Au/CeO_x/TiO_2$ (H, 1.3 nm; D, 5.9 nm)], suggesting a crucial role of the particle size in the performance of the catalysts.

Extended surfaces of Au, Cu, and Pt are not very efficient for the dissociation of water.[19,22–24] For example, DF calculations show that the partial dissociation of water ($H_2O(ads) \rightarrow OH(ads) + H(ads)$) on Cu(111) is an endothermic process ($\Delta E = 0.2-0.6$ eV) with a large activation energy ($E_a = 0.9-1.4$ eV).[19,24,46] Our DF calculations for the dissociation of water on the $Ce_2O_3/TiO_2(110)$ system of Figure 4 showed an exothermic process ($\Delta E = -0.7$ eV) with a very small activation energy ($E_a = 0.04$ eV). The final geometry of the [H + OH]/$Ce_2O_3/TiO_2(110)$ system is shown in Figure 12. In photoemission experiments, we saw the facile dissociation of water at 300 K on $CeO_x/TiO_2(110)$ surfaces in which 10−15% of the titania was precovered with CeO_x nanoparticles. The increase in the stability of the Ce^{3+} oxidation state leads to an enhancement in the chemical and catalytic activity of the ceria nanoparticles. The $M/CeO_x/TiO_2(110)$ are bifunctional catalysts: The adsorption and dissociation of water take place on the oxide, CO adsorbs on the admetal nanoparticles, and all subsequent reaction steps occur at the oxide−admetal interface. The interaction of an OH group bound on the oxide and a CO molecule bound on a metal site easily can lead to the formation of a HO−CO intermediate,[20,29] which does not have the high stability of a formate or a carbonate[19,22,24] and, therefore, is ideal for the subsequent generation of CO_2 and H_2.

The results in Figures 10 and 11 illustrate the tremendous impact that a tuning or optimization of the chemical properties of nanoceria can have on the activity of a WGS catalysts. Powder catalysts of ceria-modified titania can be prepared for practical applications.[6] The key issue is to take advantage of the complex interactions that occur in a mixed-metal oxide at a nanometer level. The titania substrate imposes on the ceria nanoparticles nontypical coordination modes, enhancing their chemical reactivity. This phenomenon leads to a larger dispersion of supported metal nanoparticles and makes possible the direct participation of the oxide in catalytic reactions.

Summary and Conclusions

At small coverages of ceria on $TiO_2(110)$, the CeO_x nanoparticles have an unusual coordination mode which favors a +3 oxidation state. Scanning tunneling microscopy and density-functional calculations point to the presence of Ce_2O_3 dimers, which are located between the rows of bridging oxygens in $TiO_2(110)$ and form diagonal arrays that have specific orientations of 0, 24, and 42° with respect to the [1 −1 0] direction of the titania substrate. At high coverages of ceria on $TiO_2(110)$, the surface exhibits two types of terraces. In one type, one has a morphology that is not very different from that observed at low ceria coverage with diagonal arrays of ceria dimers. However, in the second type of terrace, there is a compact array of ceria particles with structures that do not match the structures of $CeO_2(111)$ or $CeO_2(110)$.

CeO_x nanoparticles drastically affect the growth mode of metals on $TiO_2(110)$. At 300 K, metal adatoms do not migrate on $CeO_x/TiO_2(110)$ to create large particles in the steps; instead they are trapped at CeO_x sites in the terraces. Annealing to 625 K induces some sintering, but metal particles remain attached to CeO_x sites. Gold, copper, and platinum exhibit a quite different dispersion on the $CeO_x/TiO_2(110)$ surfaces after annealing, with the average height and diameter of the metal particles increasing in the following order: Pt < Cu < Au.

The $M/CeO_x/TiO_2(110)$ surfaces display an extremely high catalytic activity for the WGS reaction. The catalytic activity increases following the sequence $Au/CeO_x/TiO_2(110) < Cu/CeO_x/TiO_2(110) < Pt/CeO_x/TiO_2(110)$. For low coverages of Cu and CeO_x, $Cu/CeO_x/TiO_2(110)$ is 8−12 times more active than Cu(111) or Cu/ZnO industrial catalysts. In the $M/CeO_x/TiO_2(110)$ systems, there is a strong coupling of the chemical properties of the admetal and the mixed-metal oxide: The adsorption and dissociation of water probably take place on the oxide, CO adsorbs on the admetal nanoparticles, and all subsequent reaction steps occur at the oxide−admetal interface. The extremely high catalytic activity of the $M/CeO_x/TiO_2(110)$ surfaces reflects the unique properties of the mixed-metal oxide at the nanometer level.

Acknowledgment. The work performed at BNL was supported by the U.S. Department of Energy, Office of Basic Energy Sciences, under Contract DE-AC02-98CH10886. J.E. is grateful to INTEVEP and IDB for partial support of the work carried out at the UCV. The work done at Seville was funded by MICINN, Grant No. MAT2008-04918 and Barcelona Supercomputing Center—Centro Nacional de Supercomputación (Spain).

JA9087677

(44) (a) Remediakis, I. N.; Lopez, N.; Nørskov, J. K. *Appl. Catal., A* **2005**, *291*, 13. (b) Matthey, D.; Wang, J. G.; Wendt, S.; Matthiesen, J.; Schaub, R.; Laegsgaard, E.; Hammer, B.; Besenbacher, F. *Science* **2007**, *315*, 1692.

(45) Branda, M. M.; Castellani, N. J.; Grau-Crespo, R.; de Leeuw, N. H.; Hernandez, N. C.; Sanz, J. F.; Neyman, K. M.; Illas, F. *J. Chem. Phys.* **2009**, *131*, 094702.

(46) Fajín, J. L. C.; Illas, F.; Gomes, J. R. B. *J. Chem. Phys.* **2009**, *130*, 224702.